Inorganic Chemistry

ARTICLE

pubs.acs.org/IC

Thiophene Based Europium β-Diketonate Complexes: Effect of the Ligand Structure on the Emission Quantum Yield

Christelle Freund, William Porzio, Umberto Giovanella, Francesco Vignali, Mariacecilia Pasini, and Silvia Destri*

Istituto per lo Studio delle Macromolecole-CNR, Via E. Bassini 15, 20133 Milano, Italy

Agnieszka Mech

Dipartimento di Scienza dei Materiali, Università di Milano Bicocca, Via R. Cozzi 53, 20125 Milano, Italy

Sebastiano Di Pietro and Lorenzo Di Bari

Dipartimento di Chimica e Chimica Industriale, Università di Pisa, Via Risorgimento 35, 56126 Pisa, Italy

Placido Mineo

Dipartimento di Scienze Chimiche, Università di Catania, Viale A. Doria 6, 95125 Catania, Italy

Supporting Information

ABSTRACT: The synthesis and the molecular and photophysical characterization, together with solid state and solution structure analysis, of a series of europium complexes based on β-diketonate ligands are reported. The Eu(III) complex emission, specifically its photoluminescence quantum yield (PL-QY), can be tuned by changing ligands which finely modifies the environment of the metal ion. Steady-state and time-resolved emission spectroscopy and overall PL-QY measurements are reported and related to geometrical features observed in crystal structures of some selected compounds. Moreover, paramagnetic NMR, based on the analogous complexes with other lanthanides, are use to demonstrate that there is a significant structural reorganization upon dissolution, which justifies the observed differences in the emission properties between solid and solution states. The energy of the triplet levels of the ligands and the occurrence of nonradiative deactivation processes clearly account for the luminescence efficiencies of the complexes in the series.

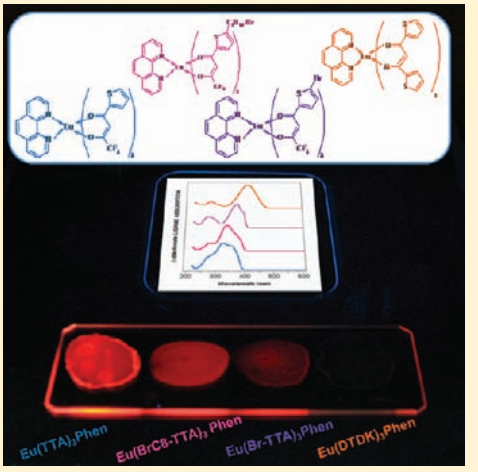

INTRODUCTION

The photophysical properties of lanthanide (Ln) complexes, based on π-conjugated ligands, acting as light antennae, have been fully assessed.[1] Interestingly the emission of ions spans from visible to IR according to the Ln(III) chosen,[1−3] allowing for applications in disparate fields such as optoelectronic devices,[1,2] sensors,[4] bioassays,[5] and telecommunication.[6] Recent years have witnessed a growing interest in their use both alone and as a component in blends with polymers imparting mechanical processing properties to the material, to fabricate organic light-emitting diodes (OLEDs) of different colors and even white OLEDs,[7] luminescent solar concentrators, lasers, and plastic optical fibers for data transmission.[8]

One of the most studied class of ligands is constituted by β-diketonate derivatives (β-DK) in view of their chemical stability, ease of preparation, and noticeable emission properties due to the effectiveness of the energy transfer (ET) from this ligand to the Ln(III) ion.[9]

Particularly, europium β-DK complexes have attracted more interest in optoelectronic applications because of their strong and narrow red emission.[8,10] The intensity of this emission depends on the type of β-diketone and on the type of complex. Considering ternary complexes of β-DK ligands and Lewis bases to complete the coordination sphere only, the majority of the highly luminescent complexes contain fluorinated groups which increase volatility and improve thermal and oxidative stability of the compounds.[11] However, a combination of aromatic and

Received: October 20, 2010
Published: May 26, 2011

Scheme 1

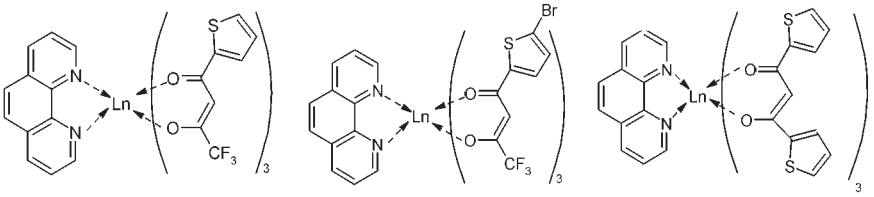

Ln(TTA)$_3$Phen Ln(Br-TTA)$_3$Phen Ln(DTDK)$_3$Phen

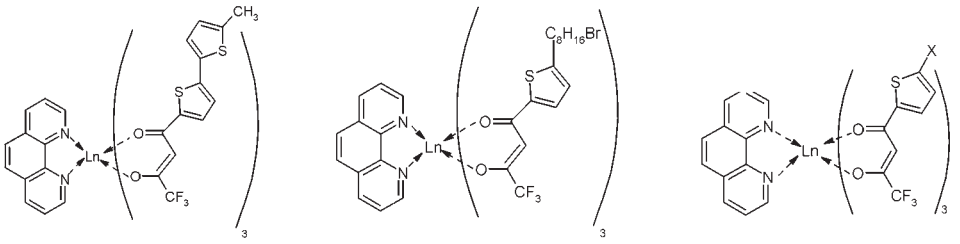

Ln(MeT-TTA)$_3$Phen Ln(BrC8-TTA)$_3$ Phen Ln(TTA)$_2$(Br-TTA)Phen
X = H in TTA; X = Br in Br-TTA

Ln =Eu, Gd, Pr, Tb, Tm, Yb, Lu

fluoro-aliphatic substituents on the diketone gives europium(III) complexes with a more intense luminescence because of the more efficient ET from the ligand to the lanthanide ion.[9b] As a matter of fact, europium tris(2-thienoyltrifluoroacetonate)·phenantroline [Eu(TTA)$_3$Phen] is one of the most efficient europium complexes in the β-DK series. To date, the largest solid state photoluminescence quantum yield (PL-QY) measured for a Eu(III) complex, [Eu(TTA)$_3$DBSO] where DBSO = dibenzyl sulfoxide, is 85%.[12] It is well-known that complex PL-QY upon ligand excitation results from a balance between the ligands-to-Eu(III) ET rates and the $^5D_0$ radiative and nonradiative decay rates. The nonradiative decay rates may have contributions from several processes: multiphonon relaxation, thermally assisted back-ET (BT) from lanthanide ion to ligand excited levels, relaxation to the ground state via crossover to another excited state, for example, the ligand-to-metal charge-transfer state of the Eu(III) ion, or ET between the lanthanide ions themselves.[13] In this contribution a series constituted by thienoyl ligands only is considered to maximize the intersystem crossing process (ISC) between S_1 and T_1 levels of the ligand (Figure 1 below). A complete characterization of these β-DK complexes, particularly the study of the PL properties in the series related to photophysical considerations, crystal structures, where available, and to complexes geometry determined by NMR studies is presented. The ligands considered in the present study are reported in Scheme 1 where Ln(III) is Eu(III) for the complexes actually discussed or Gd(III) for energy triplet determination, and Pr, Tb, Tm, Yb, Lu for paramagnetic NMR (Lu provides the necessary diamagnetic reference).

Chemical and magnetic properties of lanthanides offer a unique tool to investigate in detail the structure of these complexes in solution and to get further insight into the relation between geometry and luminescence properties. ^{1}H and ^{13}C spectra of the Eu(III) complexes do not lend themselves to an accurate analysis because of the limited pseudocontact shifts induced by Eu(III). Fortunately, taking advantage also of nuclear relaxation rates, we can demonstrate isostructurality in solution upon substitution of Eu(III) with late lanthanides, notably Tb(III) and Yb(III), which induce much larger paramagnetic shifts and derive a set of reliable pseudocontact terms, which allows us to put forward an alternative structure and dynamic picture for the complexes in solution, accounting for the PL-QY differences observed between solid and solution states.

As a consequence, the relevance of emission quenching provoked by high energy C−H oscillators in this series, although its effectiveness is lesser than that observed in Nd(III), Er(III) complexes,[14] has been recognized.

EXPERIMENTAL SECTION

Materials. Sodium amide, sodium methoxide, methanol, tetrahydrofuran (THF), ethanol, hexane, dichloromethane (CH_2Cl_2), chloroform ($CHCl_3$), ethyl ether (Et_2O), ethyl acetate, sodium hydroxide, anhydrous sodium sulfate, hydrochloric acid, and phosphoric acid were purchased from Aldrich and Merck, and deuterochloroform ($CDCl_3$) and dideuteromethylenchloride (CD_2Cl_2) from Cambridge Isotope Laboratories-Inc. Methanol, ethanol, and THF were purified by standard distillation methods.

4,4,4-Trifluoro-1-(2-thienyl)-1,3-butanedione (HTTA), 2-acetyl-3-bromothiophene, 2-acetylthiophene, 2-bromothiophene, ethyltrifluoroacetate, 2-thiophenecarboxylic acid ethyl ester, 5-(2-methylthiophene)-4,4,5,5-tetrametyl-1,3,2-dioxoborolane, 1,8-dibromooctane, acetic anhydride, tetrakis(triphenylphosphine)palladium [Pd(PPh$_3$)$_4$], 1,10-phenantroline (Phen), and europium(III) chloride hexahydrate ($EuCl_3 \cdot 6H_2O$) were purchased from Aldrich and used without any further purification. The synthesis of ligands is reported in the Supporting Information.

Apparatus and Procedure. Crystals suitable for X-ray diffraction (XRD) analysis were obtained by slow crystallization from THF for Eu(DTDK)$_3$Phen and from $CHCl_3$ for Eu(Br-TTA)$_3$Phen and

dx.doi.org/10.1021/ic1021164 |*Inorg. Chem.* 2011, 50, 5417–5429

Table 1. Crystallographic Details of Eu(Br-TTA)$_3$Phen and Eu(DTDK)$_3$Phen Complexes

chemical formula	$C_{36}H_{17}Br_3EuF_9N_2O_6S_3$	$C_{53}H_{45}EuN_2O_8S_6$
formula weight	1232.39	1182.23
space group	$P\bar{1}$ (No.2)	$P2_1/c$ (No.14)
a/nm	0.9804(1)	1.2039(8)
b/nm	1.3673(2)	3.0280(2)
c/nm	1.6067(2)	1.4916(11)
α (deg)	95.118(3)	90.0
β (deg)	95.479(3)	93.89(4)
γ (deg)	98.792(3)	90.0
V/nm^3	2106.9(5)	5425.0(15)
Z	2	4
D_{calc}/g cm^{-3}	1.943	1.447
radiation	Mo Kα (0.71073 Å)	Mo Kα (0.71073 Å)
μ/cm^{-1}	4.568	1.44
F(000)	1184	2400
temperature/ K	293	293
anomalous dispersion	all non-H atoms	all non-H atoms
parameters refined in full-matrix least-squares	541	632
unweighted agreement factor	0.057	0.058
weighted agreement factor	0.156	0.122
goodness of fit[a]	1.016	0.965
least-squares weights	b	c
largest shifts	0.00	0.05 σ
high and low peaks in final diff. map/e Å	2.77 and −1.09	0.75 and −0.53
crystal color	yellow	yellow
crystal shape	prism	prism
crystal dimensions/mm^3	0.44 × 0.25 × 0.19	0.50 × 0.23 × 0.20
instrument	Bruker-AXS SMART-APEX	Bruker-AXS SMART-APEX
empirical absorption	0.24−0.48	0.53−0.76
maximum θ/deg	25	25
reflections included $F_o > 4\sigma(F_o)$	5711 over 7406	4495 over 9524
monochromator graphite crystal, attenuator Zr foil, factor 17.0		
scan type ω	ω	ω
scan rate	10 s/image[d]	10 s/image[d]
scan width/deg	0.2	0.2

[a] Minimization function $\Sigma w(F_o^2 - F_c^2)$. [b] $w = 1/[\sigma^2(F_o^2) + (0.1125P)^2 + 2.6021P]$ where $P = (F_o^2 + 2F_c^2)/3$. [c] $w = 1/[\sigma^2(F_o^2) + (0.0723P)^2 + 0.0000P]$ where $P = (F_o^2 + 2F_c^2)/3$. [d] That is, 0.02°/s.

Eu(MeT-TTA)$_3$Phen, respectively. XRD experiments were carried out using an Enraf Nonius CAD4 instrument for single crystal analysis, while films and powder were examined using a computer controlled Siemens D-500 diffractometer equipped with Soller slits and an Anton-Paar camera for variable temperature experiments under nitrogen atmosphere.

Crystal structure resolution was performed according to the conditions shown in Table 1 and Supporting Information, Table S2, using WINGX package.[15]

NMR spectra were recorded on Bruker Advance 400 and 270 spectrometers and on a Varian Inova 600 (14.1 T) instrument equipped with triple resonance gradient probe.

FTIR spectra were taken on a Perkin-Elmer 2000 FTIR spectrometer.

Positive MALDI-TOF mass spectra were acquired by a Voyager DE-STR (PerSeptive Biosystem) using a delay extraction procedure (25 kV applied after 2600 ns with a potential gradient of 454 V/mm and a wire voltage of 25 V) and detection in linear mode. The instrument was equipped with a nitrogen laser (emission at 337 nm for 3 ns) and a flash AD converter (time base 2 ns). *trans*-2[3-(4-*tert*-Butylphenyl)-2-methyl-2-propenylidene]-malononitrile (DCTB) or dithranol were used as a matrix. Mass spectrometer calibration was performed using 5,15-bis(*p*-dodecanoxyphenyl)-10,20-bis(*p*-hydroxyphenyl)porphyrin ($C_{68}H_{78}N_4O_4$, 1014 Da) and tetrakis(*p*-dodecanoxyphenyl) porphyrin ($C_{92}H_{126}N_4O_4$, 1350 Da).

UV−vis absorption spectra for both solutions and films were measured with a Lambda 900 Perkin-Elmer spectrometer. Steady-state photoluminescence (PL) spectra were recorded using a SPEX 270 M monochromator equipped with a N_2-cooled CCD detector, by exciting with a monochromated Xe lamp. The overall PL-QY were measured in CH_2Cl_2 solution [10^{-5} Mol L^{-1}] at room temperature with respect to a reference solution of quinine sulfate in 1 N H_2SO_4 and exciting at 350 nm (PL-QY = 54.6%). The overall PL-QY for the films obtained by spin-coating from CH_2Cl_2 solutions, was determined under ligand excitation (360 nm) and is based on the absolute method using a calibrated integrating sphere.[16] The estimated error for the solid-state PL-QY is 10%.

The emission lifetimes were collected while monitoring 615 nm Eu(III) $^5D_0$-$^7F_2$ hypersensitive transition. All the samples were excited with a beam of 355 nm Nd:YAG laser, with the power of 100 μW and the repetition rate of 200 Hz (for the sample with the shorter lifetime the repetition rate was 3000 Hz), a PCI plug-in multichannel scaler ORTEC

dx.doi.org/10.1021/ic1021164 |*Inorg. Chem.* 2011, 50, 5417–5429

9353 100-ps Time Digitizer/MCS has been used in a photon counting acquisition mode, with a time resolution better than 100 ns. The estimated error for the solution emission lifetimes is 2%.

Synthesis of Complexes: General Procedure. *Eu(DTDK)$_3$Phen.* 1,3-Di(thien-2-yl)propane-1,3-dione (**HDTDK**) (708.9 mg, 3 mmol) and Phen (180.2 mg, 1 mmol) were dissolved in hot EtOH (7 mL). To this solution cooled to room temperature was added an aqueous NaOH solution (3 mL, 1 mol L^{-1}, 3 mmol). After stirring for 20 min, $EuCl_3 \cdot 6H_2O$ (366.2 mg, 1 mmol) in water (7 mL) was added to the solution. The addition was accompanied by a large precipitation. The mixture was then heated for 3 h at 60 °C. After cooling to room temperature, the yellow precipitate was collected by filtration and dried under vacuum to afford 91% of the complex (0.9437 g).

FT-IR [film from CH_2Cl_2, ν (cm^{-1})]: 1585, 1560, 1545, 1530, 1515, 1480, 1430−1410 (br), 1345, 1295 (br), 1235, 1195, 1150, 1110, 1075, 1030, 855, 840, 875, 750, 730−710 (br), 660, 620, 590. UV−vis absorption: solution (CH_2Cl_2) λ_{max} = 272 and 373 nm; film λ_{max} = 280 and 400 nm. MALDI-TOF (matrix DCTB, *m*/*z*): main peak, [2 L Phen Eu]$^+$ 802.47; [2 L 2 Phen Eu]$^+$ 982.54; the ions were detected as M$^+$ species because of loss of a DTDK$^-$ anion fragment from the corresponding molecular species. Taking into account all the peaks present in the spectrum and their intensity, a DTDK:Phen:Eu ratio of 3:1:1 could be calculated. ^{1}H NMR (CD_2Cl_2, 400 MHz, δ_{ppm}, J_{Hz}): major form (∼ 85%): 12.95 (s br, 2H, Phen), 10.71 (d, 2H, $J_{3,4}$ = 7.6, Phen), 10.06 (s, 2H, Phen), 9.29 (d, 2H, $J_{4,3}$ = 7.6, Phen), 6.68 (d, 6H, $J_{5,4}$ = 4.8, Th), 6.20 (dd br, 6H, $J_{4,3}$ = 3.6, Th), 5.59 (d, 6H, $J_{3,4}$ = 2.8, Th), 2.96 (s, 3H, CH β-diketonate); minor form (∼15%): 12.05 (s br, 2H, Phen), 10.63 (d, 2H, $J_{3,4}$ = 7.6, Phen), 9.99 (s, 2H, Phen), 9.07 (d, 2H, $J_{4,3}$ = 7.6, Phen), 6.55 (d, 6H, $J_{5,4}$ = 4.4, Th), 6.07 (dd br, 6H, $J_{4,3}$ = 3.6, Th), 5.23 (s br, 6H, Th), 2.59 (s, 3H, CH β-diketonate). ^{13}C NMR (CD_2Cl_2, 100 MHz, δ_{ppm}, J_{Hz}): 181.9 (C═O), 164.4, 162.7, 149.9, 131.3, 128.1, 123.1, 122.7, 115.1, 109.3, 94.0 (CH β-diketonate), 57.9. Elemental analysis was performed for the C, H, S atoms: calc. for $EuC_{53}H_{45}O_8N_2S_6$ using crystal for XRD: C, 53.84; H, 3.84; S, 16.27. Found C, 53.72; H, 3.92; S, 16.13.

Eu(TTA)$_3$Phen. Starting products: Phen and HTTA as ligands, and $EuCl_3 \cdot 6H_2O$ as the metal precursor. The complex was obtained as a pale rose powder with a yield of 65% after crystallization from $CHCl_3$. MALDI-TOF (matrix dithranol, *m*/*z*): [2 L Phen Eu]$^+$ 773.4, main peak; [2 L 2Phen Eu]$^+$ 953.7; the ions were detected as M$^+$ species because of loss of a TTA fragment from the corresponding molecular species. Taking into account all the peaks present in the spectrum and their intensity a TTA: Phen: Eu ratio of 3:1:1 could be calculated. ^{1}H NMR (CD_2Cl_2, 400 MHz, δ_{ppm}, J_{Hz}): 10.89 (s br, 2H, Phen), 10.17 (d, 2H, $J_{4,3}$ = 8.0, Phen), 9.44 (s, 2H, Phen), 8.56 (d, 2H, $J_{3,4}$ = 7.6, Phen), 7.04 (d, 3H, $J_{5,4}$ = 4.8, Th), 6.50 (dd, 3H, $J_{4,5}$ = 4.2, Th), 6.02 (s large, 3H, Th), 3.13 (s, 3H, CH β-diketonate). ^{13}C NMR (CD_2Cl_2, 100 MHz, δ_{ppm}, J_{Hz}): 179.5 (CO-Th), 168.8 (CO−CF_3), 162.9, 150.2, 135.5, 127.1, 127.0, 123.7, 112.2, 106.3, 95.6 (CH β-diketonate). Elemental analysis was performed for C, H, S, atoms. Calc. for $EuC_{36}H_{20}F_9O_6N_2S_3$: C, 43.43 ; H, 2.02; S, 9.66. Found: C, 43.70; H, 1.92; S, 9.48.

Eu(Br-TTA)$_3$Phen. Starting products: Phen and Br-HTTA as ligands, and $EuCl_3 \cdot 6H_2O$ as the metal precursor. The complex was obtained as a light orange powder which was crystallized from $CHCl_3$ (yield 70%). MALDI-TOF (matrix dithranol, *m*/*z*): [2 L Phen Eu]$^+$ 931.3, main peak; [2 L 2Phen Eu]$^+$ 1111.4; the ions were detected as M$^+$ species, because of loss of a BrTTA$^-$ anion fragment from the corresponding molecular species. Taking into account all the peaks present in the spectrum and their intensity a Br-TTA:Phen:Eu ratio of 3:1:1 could be calculated. NMR ^{1}H (CD_2Cl_2, 400 MHz, δ_{ppm}, J_{Hz}): 10.94 (s large, 2H, Phen), 10.12 (s large, 2H, Phen), 9.35 (s, 2H, Phen), 8.53 (s large, 2H, Phen), 6.50 (s br, 3H, Th), 5.66 (s br, 3H, Th), 3.24 (s, 3H, CH β-diketonate). ^{1}H NMR (acetone d_6, 270 MHz, δ_{ppm}, J_{Hz}): 11.82 (s large, 2H, Phen), 10.21 (d, $J_{4,3}$ = 7.8, 2H, Phen), 9.28 (s, 2H, Phen), 8.69 (d, $J_{3,4}$ = 7.0, 2H, Phen), 6.50 (d, $J_{4,3}$ = 4.1, 3H, Th), 5.64 (d, $J_{3,4}$ = 4.1, 3H, Th), 3.29 (s, 3H, CH β-diketonate). ^{13}C NMR (CD_2Cl_2, 100 MHz, δ_{ppm}, J_{Hz}): 179.5 (CO-Th), 168.3 (CO−CF_3), 162.8, 150.4, 127.1, 126.7, 124.8, 111.8, 106.2, 97.5 CH β-diketonate. Elemental analysis was performed for C, H, S, atoms: Calc. for $EuBr_3S_3F_9O_6N_2C_{36}H_{17}$: C, 35.09; H, 1.39; S, 7.81. Found: C, 34.87; H, 1.43; S, 7.58.

Eu(TTA)$_2$(Br-TTA)Phen. Starting products: Phen, HTTA, and Br-HTTA as ligands and $EuCl_3 \cdot 6H_2O$ as the metal precursor, in the respective stoichiometry of 1, 2, 1, and 1. Yield 85%. The complex was obtained as a light pink beige powder, which emits strongly under excitation at 360 nm, in the solid state and in solution as well. No attempts for purification were performed, to avoid any decomposition. MALDI-TOF (matrix dithranol, *m*/*z*): [2L1 Phen Eu]$^+$ 773.6; [L1 L2 Phen Eu]$^+$ 851.5; [2L2 Phen Eu]$^+$ 931.3; [2L1 2Phen Eu]$^+$ 953.6; [L1 L2 2Phen Eu]$^+$ 1031.6; [2L2 2Phen Eu]$^+$ 1111.4; the ions were detected as M$^+$ species because of loss of a TTA$^-$ or Br-TTA$^-$ anion fragment from the corresponding molecular species. ^{1}H NMR (CD_2Cl_2, 400 MHz, δ_{ppm}, J_{Hz}): 10.88−10.82 (2H, Phen), 10.12−10.02 (2H, Phen), 9.37−9.25 (2H, Phen), 8.49−8.45 (2H, Phen), 6.96 (d, 2H, $J_{5,4}$ = 4.6, Th TTA), 6.47−6.40 [m, 3H, Th TTA (2H) and Th Br-TTA (1H)], 5.94 and 5.86 (2d, 2H, $J_{3,4}$ = 3.6, Th TTA), 5.71 and 5.63 (2d, 1H, $J_{3,4}$ = 3.8, Th Br-TTA), 3.50 and 3.28 (2s, 1H, CH β-diketonate of Br-TTA), 3.05 and 2.88 (2s, 2H, CH β-diketonate of TTA). ^{13}C NMR (CD_2Cl_2, 100 MHz, δ_{ppm}, J_{Hz}): 179.5, 168.6, 162.8, 150.2, 135.6, 135.5, 127.2, 127.1, 127.0, 126.9, 126.5, 124.5, 123.7, 123.6, 112.0, 106.2, 95.6, and 95.1 (*C*H β-diketonate). Elemental analysis was performed for C, H, S, atoms: Calc. for $EuC_{36}H_{19}BrF_9N_2O_6S_3$: C, 40.24; H, 1.78; S, 8.95. Found: C, 40.04; H, 1.88; S, 8.78.

Eu(BrC8-TTA)$_3$Phen. Starting products: Phen and BrC8-HTTA as ligands, and $EuCl_3 \cdot 6H_2O$ as the metal precursor Yield 48%. The complex was obtained as a yellowish solid after precipitation from hexane solution. MALDI-TOF (matrix dithranol, *m*/*z*): main peak [2 L Phen Eu]$^+$ 1154.9; [2 L 2Phen Eu]$^+$ 1333.7; the ions were detected as M$^+$ species, because of loss of a BrC8-TTA$^-$ anion fragment from the corresponding molecular species. Taking into account all the peaks present in the spectrum and their intensity a BrC8TTA:Phen:Eu ratio of 3:1:1 could be calculated. ^{1}H NMR (CD_2Cl_2, 270 MHz, δ_{ppm}, J_{Hz}) 10.35 (s br, 2H, Phen), 10.15 (d, 2H, $J_{4,3}$ = 8.1, Phen), 9.47 (s, 2H, Phen), 8.48 (d br, 2H, $J_{3,4}$ = 8.1, Phen), 6.14 (d, $J_{3,4}$ = 3,4, 3H, Th), 5.83 (d $J_{4,3}$, 3H, Th), 3.50 (t, 6H, CH_2−Th), 3.42 (t, 6H, CH_2−Br), 2.47 (s, 3H, CH β-diketonate), 1.89−1.26 (36H, alkyl chain). Elemental analysis was performed for C, H, S, atoms: Calc. for $EuC_{60}H_{65}F_9N_2O_6S_3Br_3$: C, 45.93 ; H, 4.18; S, 6.13. Found: C, 46.03 ; H, 4.01; S, 6.00.

Eu(MeT-TTA)$_3$Phen. Starting products: Phen and MeT-HTTA as ligands, and $EuCl_3 \cdot 6H_2O$ as the metal precursor. Solvent EtOH:THF (1:5). The complex was obtained as a yellow powder with a yield of 72% after crystallization from $CHCl_3$. MALDI-TOF (matrix dithranol, *m*/*z*): [2 L Phen Eu]$^+$ 965.57; [3 L Eu]H$^+$ 1102.26; the ions were detected as M$^+$ species, because of loss of a MeT-TTA$^-$ anion fragment from the corresponding molecular species, and as MH$^+$ species, respectively. Taking into account all the peaks present in the spectrum and their intensity a MeT-TTA:Phen:Eu ratio of 3:1:1 could be calculated. ^{1}H NMR (CD_2Cl_2, 270 MHz, δ_{ppm}, J_{Hz}): 11.09 (s br, 2H, Phen), 10.06 (d, 2H, $J_{4,3}$ = 7.8, Phen), 9.31 (s, 2H, Phen), 8.53 (d, 2H, $J_{3,4}$ = 7.6, Phen), 7.26 (d, 3H, J = 3.2, Th), 6.90 (d, 3H, J = 2.4, Th), 6.45 (d, 3H, J = 3.8, Th), 5.76 (d, 3H, J = 3.8, Th), 2.97 (s, 3H, CH β-diketonate), 2.73 (s, 9H, Me). Elemental analysis was performed for C, H, S, atoms: Calc. for $EuC_{51}H_{32}F_9N_2O_6S_6$: C, 47.70; H, 2.51; S, 14.98. Found C, 47.82; H, 2.55; S, 14.80.

The same synthetic procedures were used in the preparation of the corresponding Ln(TTA)$_3$Phen, Ln = Gd, Pr, Tb, Tm, Yb, Lu, as well as for the systems of empirical formula Gd(Br-TTA)$_3$Phen, Gd(TTA)$_2$-(Br-TTA)Phen, Gd(BrC8-TTA)$_3$Phen, Gd(DTDK)$_3$Phen, Yb (TTA)$_2$-(Br-TTA)Phen, and Yb(BrC8-TTA)$_3$Phen. Elemental analyses were performed for C, H, S, atoms:

dx.doi.org/10.1021/ic1021164 |*Inorg. Chem.* 2011, 50, 5417–5429

Calc. for $GdC_{36}H_{20}F_9N_2O_6S_3$: C, 43.20; H, 2.01; S, 9.61. Found C, 43.47; H, 2.12; S, 9.44.
Calc. for $GdBr_3S_3F_9O_6N_2C_{36}H_{17}$: C, 34.97; H, 1.39; S, 7.78. Found: C, 34.80; H, 1.43; S, 7.55.
Calc. for $GdC_{36}H_{19}BrF_9N_2O_6S_3$: C, 40.06; H, 1.77; S, 8.91. Found: C, 39.93; H, 1.85; S, 8.72.
Calc. for $GdC_{60}H_{65}F_9N_2O_6S_3Br_3$: C, 45.81; H, 4.16; S, 6.11. Found: C, 45.93; H, 4.21; S, 6.00.
Calc. for $GdC_{53}H_{45}O_8N_2S_6$: C, 53.60; H, 3.82; S, 16.20. Found C, 53.49; H, 3.94; S, 16.01.
Calc. for $PrC_{36}H_{20}F_9N_2O_6S_3$: C, 43.91; H, 2.05; S, 9.77. Found C, 44.12; H, 2.15; S, 9.58.
Calc. for $TbC_{36}H_{20}F_9N_2O_6S_3$: C, 43.12; H, 2.01; S, 9.59. Found C, 43.30; H, 2.13; S, 9.40.
Calc. for $TmC_{36}H_{20}F_9N_2O_6S_3$: C, 42.70; H, 1.99; S, 9.50. Found C, 42.85; H, 2.07; S, 9.37.
Calc. for $YbC_{36}H_{20}F_9N_2O_6S_3$: C, 42.52; H, 1.98; S, 9.46. Found C, 42.72 ; H, 2.09; S, 9.26.
Calc. for $LuC_{36}H_{20}F_9N_2O_6S_3$: C, 42.44; H, 1.98; S, 9.44. Found C, 42.63; H, 2.08; S, 9.27.
Calc. for $YbC_{36}H_{19}BrF_9N_2O_6S_3$: C, 39.46; H, 1.75; S, 8.78. Found: C, 39.60; H, 1.88; S, 8.59.
Calc. for $YbC_{60}H_{65}F_9N_2O_6S_3Br_3$: C, 45.32; H, 4.12; S, 6.05. Found: C, 45.54; H, 4.01; S, 5.91.

RESULTS AND DISCUSSIONS

Synthesis of Ligands and Complexes. 5-Bromo-2-thienoyltrifluoroacetone Br-HTTA was synthesized by the Claisen condensation of 2-acetyl-5-bromothiophene and ethyltrifluoroacetate with sodium methoxide as the base and MeOH/Et_2O mixture as the solvent.[17] The pure product was obtained in a 65% yield after sublimation. In the synthesis of ligand HDTDK, sodium amide replaced sodium methoxide as the base, and THF was used as the solvent.[18] To obtain MeT-HTTA the strategy of modifying the acetylthiophene reagent via Suzuki coupling was adopted. Specifically 5-bromo-2-acetylthiophene reacted with the 5-(2-methylthiophene)-boronic acid pinacol ester to afford the intermediate ketone, which was later transformed by a Claisen type condensation with ethyltrifluoroacetate, into the corresponding diketone MeT-HTTA. 8-Bromooctyl-2-thienoyltrifluoroacetone (BrC8-HTTA) was prepared by acylation with acetic anhydride and phosphoric acid[19] of 2-(8-bromooctyl)thiophene, obtained following the procedure reported in the literature,[20] and subsequent Claisen condensation of ethyltrifluoroacetate on the terminal ketonic group.[17] NMR spectroscopy of the β-DK ligands in $CDCl_3$ as the solvent shows the presence of both ketonic and enolic tautomers for HDTDK, BrC8-HTTA, and Br-HTTA, although in a different ratio (15% for the first, 10% for the second, and less than 1% for the third one, this last percentage slightly increases in a more polar solvent as deuterated acetone); while for MeT-HTTA as well as for HTTA only the signal of enolic form is apparent. The stronger push−pull character of the latter group of molecules can be related to the enolic form stabilization.[21]

The complexes Eu(Ligand)$_3$Phen were synthesized from $EuCl_3 \cdot 6H_2O$ and the corresponding diketonate in EtOH/water with phenanthroline as the ancillary ligand as described by Melby et al.[22] and reported in Scheme 2.

In the case of 5-methylthien-2-yl, higher yields of complex were attained only by using 1:5 EtOH:THF as the solvent, to maintain the ligand enolic anion in solution. The complexes are poorly soluble in most organic solvents except for acetone. They are partially soluble in CH_2Cl_2, $CHCl_3$, and EtOH. The complexes were characterized by ^1H, ^{13}C NMR spectroscopy, (see also below results and discussion on paramagnetic NMR). ^{13}C NMR spectrum was carried out only in the case of adequate solubility of the complex. FTIR and UV−vis spectroscopy, cyclovoltammetry (presented in Supporting Information, Table S1 and Figure S1), elemental analysis, MALDI-TOF mass spectrometry determination together with XRD analysis, when single crystals could be obtained, were performed to complete the characterization. The two last analyses and NMR integrals are in agreement with a Ligand:Phen:Ln ratio of 3:1:1. In the MALDI-TOF experiments, in some cases, exchanges among the ligands was observed, and also the matrix taking part in this process. Deeper investigations are in progress with different matrixes to clarify the matrix effect and will be the object of a forthcoming paper.

Photophysical Characterization. The optical properties of Eu(III) complexes have been studied for both CH_2Cl_2 diluted solutions and solid-state (thin film) samples by absorption, steady-state and time-resolved emission spectroscopy, and overall PL-QY measurements.

In Figure 1, the absorption spectra of the ligands in solution (a) and of all the complexes in solution and as thin film (b) are shown. The broad bands of the ligand absorption show their maximum (λ_{max}) ranging from 250 to 375 nm and absorption edges up to 430 nm. The exception being MeT-HTTA whose λ_{max} is equal to 415 nm. The absorption profiles of the complexes dominated by the ligand absorption are almost identical for the samples measured in solution as well as in thin films. As expected the edge of the absorption band for the thin films is slightly red-shifted.

The sensitization pathway in Ln(III) complexes generally consists of excitation of the ligand into its singlet excited state, subsequent ISC to its triplet state, and ET from the triplet state of the ligand to the Ln(III) ion.[1,5a,9b]

To determine the energy of the triplet state of the ligands versus energy states of Eu(III) ions, the phosphorescence spectra of the frozen solution of the corresponding Gd^{3+} complexes,

Scheme 2

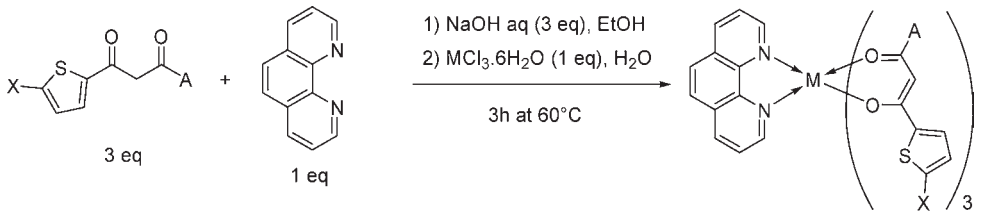

A= CF_3, thien-2-yl and X = H, Br, 5-methylthien-2-yl, $C_8H_{16}Br$

dx.doi.org/10.1021/ic1021164 |Inorg. Chem. 2011, 50, 5417–5429

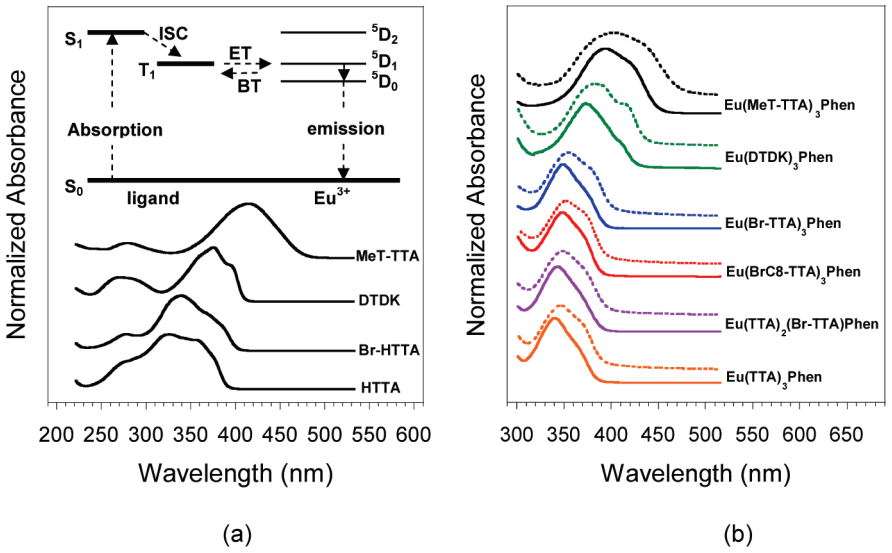

Figure 1. Normalized Absorbance of ligands in CH_2Cl_2 solution [10^{-5} mol·L^{-1}] (a), Eu(III) complexes (b) in CH_2Cl_2 solution [10^{-5} mol·L^{-1}] (solid-line) and in film (dotted-line). In the inset, diagram of the most probable states involved in the photophysics of the Eu(III) complexes.

considering the 0−0 transition, were measured[7b] (Supporting Information, Figure S2). The energy values of the triplet levels of the ligands in complexes were as follows: TTA (502 nm, 19920 cm^{-1}), BrC8-TTA (511 nm, 19569 cm^{-1}), and Br-TTA (521 nm, 19194 cm^{-1}), which places them between the $^5D_2$ (465 nm, 21500 cm^{-1}) and $^5D_1$ (524 nm, 19070 cm^{-1}) excited states of the metal ion.[23] As already shown by Chen et al.,[24] the introduction of an electron donor substituent on the TTA ligand provokes a bathochromic shift of the triplet state energy level. The energy of the triplet state of DTKT (531 nm, 18832 cm^{-1}) is close to the $^5D_0$ (578 nm, 17300 cm^{-1}) level of Eu(III).[2] The energy of the triplet state of the ligand MeT-TTA was hard to determine because the ligand fluorescence in the corresponding Gd(MeT-TTA)$_3$Phen frozen solution overlaps the phosphorescence, indicating that the triplet state was scarcely populated. A value around 526 nm, 19011 cm^{-1}, too close to $^5D_1$ to prevent metal−ligand BT, was estimated. A diagram of the most probable states involved in the photophysics of the Eu(III) complexes is reported as inset in Figure 1.

Figure 2 presents the emission spectra recorded for all the complexes in solution (Supporting Information, Figure S3 for PL spectra of the films). These emission spectra show typical Eu^{3+} PL features corresponding to the transitions $^5D_0 \rightarrow {}^7F_0$ (around 580 nm), $^5D_0 \rightarrow {}^7F_1$ (592 nm), the hypersensitive $^5D_0 \rightarrow {}^7F_2$ (615 nm), $^5D_0 \rightarrow {}^7F_3$ (around 635 nm), and $^5D_0 \rightarrow {}^7F_4$ (around 685 nm). The intensity of the $^5D_0 \rightarrow {}^7F_2$ transition (electric dipole) is greater than that of the $^5D_0 \rightarrow {}^7F_1$ transition (magnetic dipole) suggesting that the coordination environment of the Eu^{3+} ion is free from an inversion center. The emission spectra of Eu(III) complexes do not exhibit the ligand centered transition, signifying that there is an efficient intramolecular ET from the β-DK ligand to the Eu^{3+} ions.

It is well established in the literature that for Eu(III) β-DK complexes, the largest PL-QY is observed when the energy of the triplet state of the ligand is close to the energy of $^5D_1$ level of Eu(III) by keeping to the following phenomenological rule ΔE (T_1* − Ln* emissive level) in the range 2500−3500 cm^{-1}.[5a,25] For these reasons, high PL-QY should be expected from

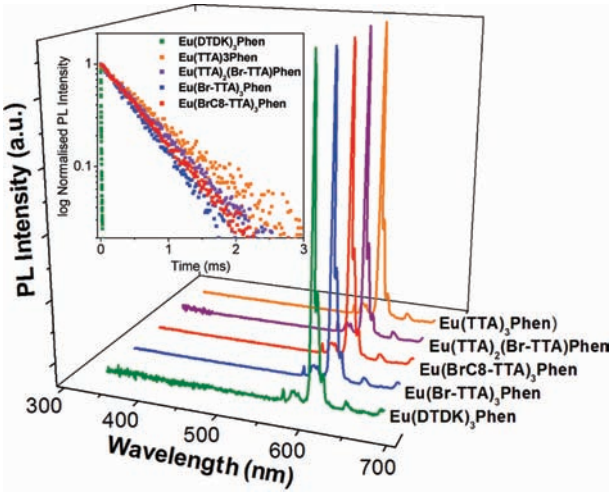

Figure 2. PL spectra of the complexes in CH_2Cl_2 solution [10^{-5} Mol L^{-1}] by exciting at 350 nm. Inset, time-resolved emission spectra of the complexes in solution.

Eu(TTA)$_3$Phen, Eu(Br-TTA)$_3$Phen, Eu(TTA)$_2$(Br-TTA)Phen, and Eu(BrC8-TTA)$_3$Phen complexes, while for Eu(DTDK)$_3$-Phen and Eu(MeT-TTA)$_3$Phen the feeding state becomes too close to the energy of the $^5D_0$ (the emitting state) and the $^5D_1$ respectively, and BT operates.

To verify this behavior, the steady-state PL-QY of solutions and films (presented in Table 2) as well as the emission decay measurements of solutions at room temperature were carried out. The recorded PL-QY values for thin film are in the range from 0.72 for Eu(TTA)$_3$Phen (which is in agreement with the value reported in literature)[26] to 0.41 for both Eu(TTA)$_2$(Br-TTA)Phen and Eu(BrC8-TTA)$_3$Phen, 0.34 for Eu(Br-TTA)$_3$Phen, down to less than 0.01 for Eu(DTDK)$_3$Phen and Eu(MeT-TTA)$_3$Phen, indicating an almost complete quenching of the emission in these latter ones.

dx.doi.org/10.1021/ic1021164 |Inorg. Chem. 2011, 50, 5417–5429

Table 2. Overall PL-QY of All the Complexes in Film and Solution [CH_2Cl_2, 10^{-5} M], the Relative Integrated Intensity of the $^5D_0 \rightarrow {}^7F_2$ Transition with Respect to That of the $^5D_0 \rightarrow {}^7F_1$ Transition Band (A_{21}), $^5D_0$ Lifetime (τ_{obs}), Radiative (A_{RAD}) and Non-Radiative (A_{NR}) Decay Rates, Intrinsic PL-QY of Eu(III) (PL-QY_{intr}), and the ET Efficiencies (η_{sens}) in Solution

	film		solution						
complex	PL-QY	A_{21}	PL-QY	A_{21}	τ_{obs} (μs)	A_{RAD} (s^{-1})	A_{NR} (s^{-1})	PL-QY_{intr}	η_{sens} (%)
$Eu(TTA)_3Phen$	0.72[a]	18.4	0.48	15.6	710	713	695	0.51	95
$Eu(TTA)_2$(Br-TTA)Phen	0.41[b]		0.43	14.7	610	736	903	0.45	96
$Eu(BrC8\text{-}TTA)_3Phen$	0.41[b]		0.43	14.9	550	748	1070	0.41	≈100
$Eu(Br\text{-}TTA)_3Phen$	0.34[a]	17.3	0.37	13.3	500	729	1271	0.36	≈100
$Eu(DTDK)_3Phen$	<0.01[a]	14.8	0.01	14.7	5	843		0	
$Eu(MeT\text{-}TTA)_3Phen$	<0.01[a]		<0.01						

[a] Semicrystalline film. [b] Amorphous film. Estimated relative errors: τ_{obs}, ± 2%; PL-QY, ± 10%; τ_{rad}, ± 10%; PL-QY_{intr}, ± 12%; η_{sens}, ± 22%.

In CH_2Cl_2 solution, the PL-QY of $Eu(TTA)_3Phen$ decreases to 0.48 as reported in the literature,[26] while the PL-QY values of the other complexes are substantially unmodified with respect to the corresponding film (Table 2).

To evaluate the efficiency of the Eu(III) sensitized emission, its 615 nm luminescence decay profiles (Figure 2 inset) were measured in solution upon excitation of the ligand absorption band at 355 nm. The PL decay profiles measured for all the samples are well fitted by a single-exponential function, which indicates that the Eu(III) ions are placed in a unique symmetry site with a lifetimes (τ_{obs}) in the range 0.50−0.71 ms (see Table 2), typical for Eu(III) organic complexes with β-DKs.[27] Such a long τ_{obs} is, however, not observed for $Eu(DTDK)_3Phen$ that exhibits 0.005 ms lifetime (i.e., strong emission quenching). It is worth to underline that the trend observed for transient decays in the solutions is the same as for PL-QY.

The ligands must protect Eu(III) from the external sources of nonradiative deactivation (like water and solvents molecules), and provide efficient light harvesting and ligand-to-metal ET (η_{sens}) to achieve high PL-QY values. To get a better understanding of the radiative and nonradiative pathways, the PL efficiencies of Eu(III) complexes in solution are analyzed in terms of the equation[8b,28]

$$\text{PL-QY} = \eta_{sens} \times \text{PL-QY}_{intr} = \eta_{sens} \times \left(\frac{\tau_{obs}}{\tau_{rad}}\right)$$

where PL-QY_{intr} is the intrinsic PL-QY of Eu(III), η_{sens} is the efficiency of the ligand-to-metal ET, and τ_{obs} and τ_{rad} are the observed and the radiative lifetimes. The details of the calculations were reported in ref 28.

The overall PL-QY, the relative integrated intensity of the $^5D_0 \rightarrow {}^7F_2$ transition with respect to that of the $^5D_0 \rightarrow {}^7F_1$ transition band (A_{21}), the radiative (A_{RAD}) and nonradiative (A_{NR}) decay rates, and η_{sens} for all complexes in solution are presented in Table 2.

Because of the extremely fast emission transient decay and very low PL-QY of the $Eu(DTDK)_3Phen$, the calculated values of η_{sens} and A_{NR} are senseless. The very low PL-QY of this complex is probably related to inefficient intramolecular ET between ligand and metal ion caused by the very low energy of the triplet state of DTDK.

On the contrary, all the remaining complexes exhibit the same high η_{sens} as the $Eu(TTA)_3Phen$ suggesting that the matching differences between the energy of the triplet level of the ligand and the $^5D_1$ energy level of the Eu(III) ion cannot be applied as a simple explanation, and nonradiative decay mechanisms must be taken into consideration. Indeed the nonradiative deactivation rates are two times higher for all the complexes than the one calculated for $Eu(TTA)_3Phen$.

In Table 2 the PL-QY measured on a films of all the samples are reported too. As already mentioned an increase of the value related to $Eu(TTA)_3Phen$ complex with respect to that one of solution is observed. Paramagnetic NMR analysis clearly indicates an augmented molecular symmetry in solution as compared with solid state (cf. XRD and NMR data below).

As the magnetic-dipole transitions $^5D_0 \rightarrow {}^7F_1$ are nearly independent of the ligand field, they can be used as an internal standard to account for ligand differences.[29] The electric-dipole transitions $^5D_0 \rightarrow {}^7F_2$, are sensitive to the symmetry of the coordination sphere. The A_{21} ratio in the lanthanide complex measures the symmetry of the coordination sphere.[30]

In the solid state the distortion of the symmetry around the Eu(III) ion enhances the probability of the electric-dipole transition implying increased PL-QY values. Moreover, PL-QY depends on the η_{sens} values which are in their turn related to the distance of the Eu ligands.[1] Considering that the intramolecular ligand-to-Eu ET are almost complete in solution and the ligand−metal distances vary less than 0.01 nm in the solid state for all the TTAs complexes (see below), the variation of η_{sens} should not influence PL-QY in our case. Indeed the PL-QY increment is verified for $Eu(TTA)_3Phen$ only. The deactivation processes already evidenced in solution must take place in the solid state too and are probably even more important.

Although OH oscillators, for example, as in bound water molecules, are the most effective quenchers both in the solid state and in solution, clear evidence for the quenching effect of higher harmonics of N−H, C−H and C═O, which are less efficient oscillators, is provided;[31] thus, a deeper analysis of the possible deactivation processes has to be performed.

To give further insight into the quenching processes, specifically to justify the trend observed for PL-QY and the lifetime of the complexes, structural determinations both in solid state and in solution have been carried out. The geometry of the complexes has been compared with that of other complexes whose crystallographic data are reported in the literature.

Crystal Structures of $Eu(Br\text{-}TTA)_3Phen$ and $Eu(DTDK)_3Phen$. The crystal and molecular structures of three Eu(III) complexes of the series were solved. We report here data related to $Eu(Br\text{-}TTA)_3Phen$ and $Eu(DTDK)_3Phen$, while the data for $Eu(MeT\text{-}TTA)_3Phen$ are provided in the Supporting Information in view of the mosaic spread of the crystals, preventing

dx.doi.org/10.1021/ic1021164 |Inorg. Chem. 2011, 50, 5417–5429

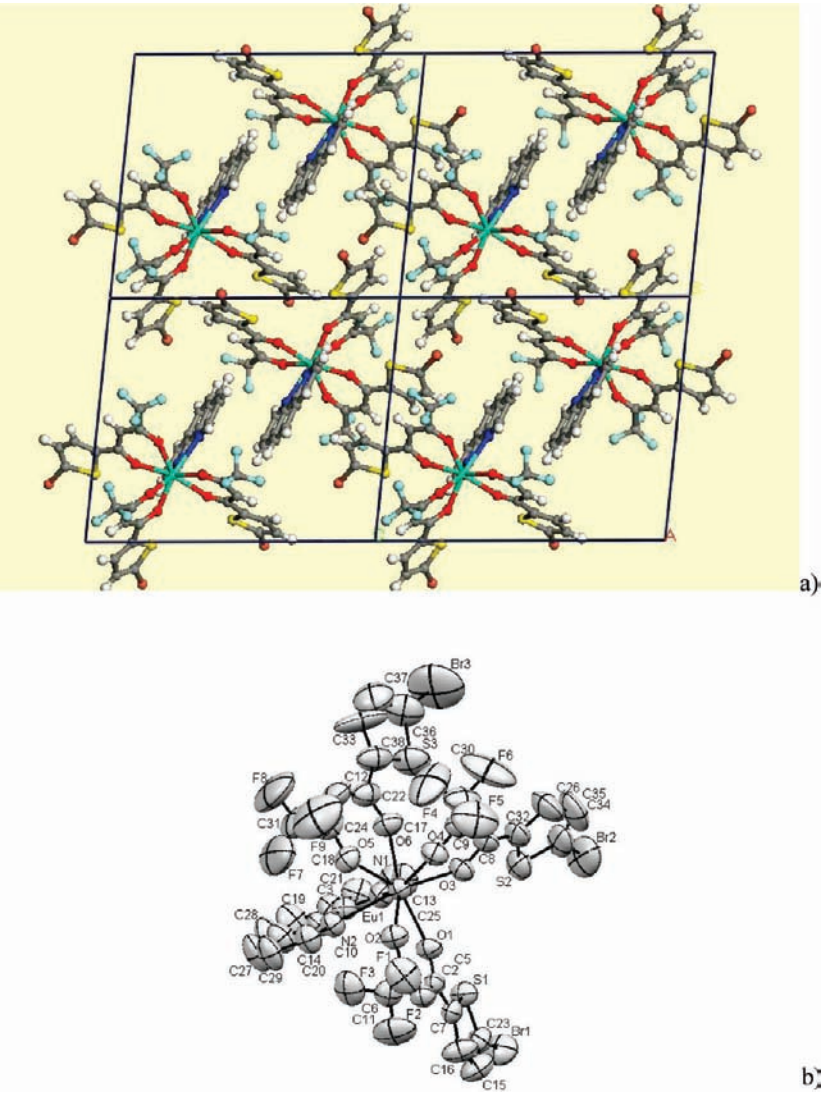

Figure 3. (a) *a* axis view of the crystal packing of Eu(Br-TTA)$_3$Phen complex; (b) ORTEP plot with thermal ellipsoid probability of 50%.

accurate crystal structure refinement. All of them are characterized by quite expected geometries on the basis on the crystallographic findings of the archetype complex, that is, Eu(TTA)$_3$-Phen crystal.[32] The main features of the crystal data and the structural resolution are reported in Table 1, while in Figure 3 and 4 the corresponding crystal packings are shown.

The octa-coordination at Eu-atom is quite distorted, namely, instead of the expected value of 180°, the average plane of two opposite β-DK forms an angle ranging from ∼164° for Eu-(DTDK)$_3$Phen to 151° for Eu(Br-TTA)$_3$Phen and to 146° for Eu(MeT-TTA)$_3$Phen, while the corresponding angle between Phen and the remaining β-DK residue is contracted from ∼146° in Eu(DTDK)$_3$Phen to ∼140° in Eu(Br-TTA)$_3$Phen or constant (151°) in Eu(MeT-TTA)$_3$Phen. The different packing arrangement motif in these three crystals is clearly attributed to the presence of a solvent molecule, completely confirmed in the crystal structure of the parent complexes Eu(TTA)$_3$(Phen)[32] and Eu(TTA)$_3$BipyCO,[33] namely, in the latter case a toluene molecule is present.

Specifically, in the absence of any clathrated molecule the crystal packing consists in the facing of adjacent Phen ligands allowing for a Eu−Eu separation over 0.9 nm (Table 3 below). Conversely when solvent molecules are included into the crystal, Phen molecules cannot face, adjacent β-DK residues partially overlap, and a remarkable reduction of the packing factor occurs, namely, in crystals of Eu(DTDK)$_3$Phen the packing factor value drops to 0.62 to be compared with the close packed crystal value (≥0.7).

Comparison of Structures of Eu(III) Complexes. To shed light onto photophysical properties observed in the series of Eu(III) complexes containing thiophene β-DK and Phen ligands, shown in Scheme 1, some structural features were taken into account and compared, for example, the shortest metal−metal distances, the europium-ligand distances, and the angle formed by EuOO and β-DK residues planes in the crystals considered. All these values are reported in Table 3. A more complete analysis including crystal structures of complexes containing bisphenyl-(1,3-β-diketonate) and bipyridyl ligand is reported in the Supporting Information.

The closest Eu−Eu distances range from 0.893 to 1.054 nm (see line 4 of Table 3); this fact implies that the metal−metal interaction, possibly contributing to quenching the emission, cannot be accounted for as the main parameter affecting the

dx.doi.org/10.1021/ic1021164 |*Inorg. Chem.* 2011, 50, 5417–5429

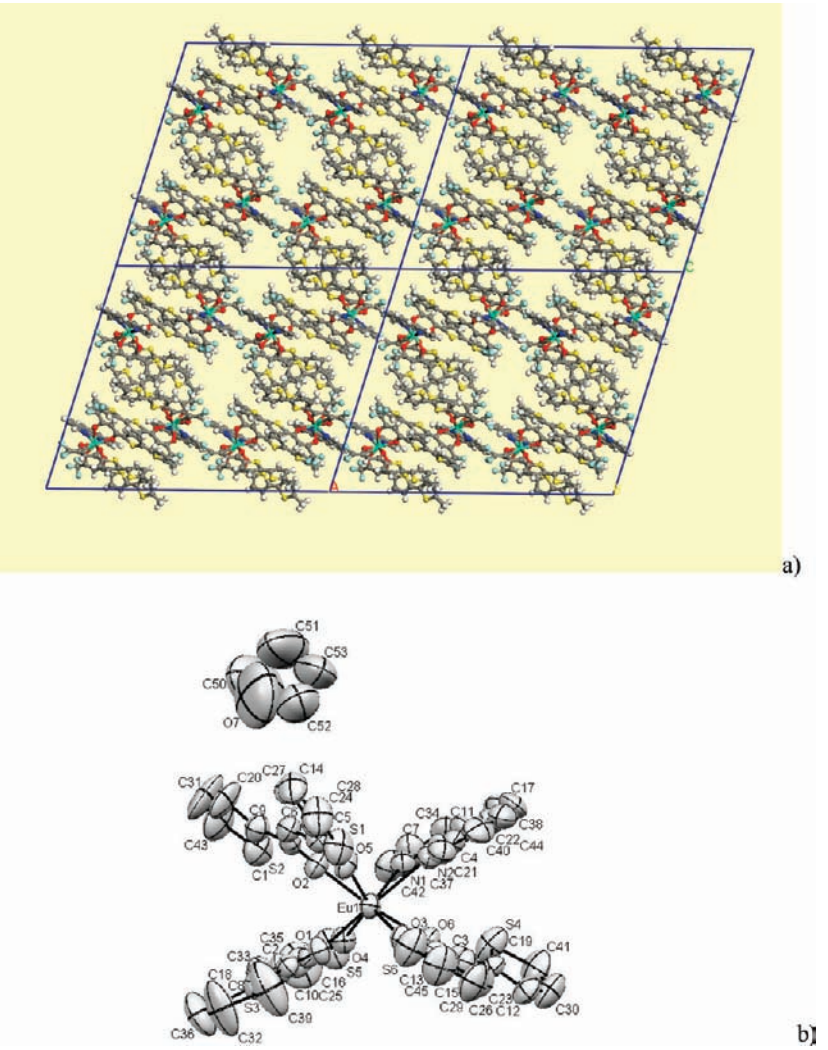

Figure 4. (a) Crystal packing of Eu(DTDK)$_3$Phen complex, viewed along *b* axis; (b) ORTEP plot with thermal ellipsoid probability of 50%.

Table 3. Comparison among Eu−O, Eu−N, and Eu−Eu Distances (nm) in Eu(III) Complexes with Phenanthroline and Thiophene *β*-DK Ligands, Together with the Angles (deg) Formed by EuOO and *β*-DK Residue Planes in the Crystals of the Considered Complexes

	complex			
geometric parameter	Eu(TTA)$_3$Phen	Eu(Br-TTA)$_3$Phen	Eu (DTDK)$_3$Phen[a]	Eu(MeT-TTA)$_3$Phen[b]
average Eu−O distance crystal esd ≤0.0016 nm	0.2362	0.2359	0.2357	0.2628
average Eu−N distance crystal esd ≤0.0010 nm	0.2594	0.2594	0.2628	0.2572
shortest Eu−Eu distance crystal esd ≤0.0010 nm	0.976	0.980	0.893	1.054
EuOO−*β*-DK1	12	21	20	20
EuOO−*β*-DK2	1	≥1	6	≥2
EuOO−*β*-DK3	≤2	3	14	17

[a] Two tetrahydrofuran molecules are clathrated in the crystal. [b] Because of the low quality of the crystals, the values are affected by a large esd of 0.005.

emission properties. As a matter of fact, an energy minimization calculation, using the COMPASS program of the MATSTUDIO package,[34] on Eu(BrC8-TTA)$_3$Phen molecule, whose bulky ligands allow for larger metal separation, gives values ranging from 1350 to 1400 kcal/mol by varying the Eu−Eu distances from 0.95 to 1.7 nm.

dx.doi.org/10.1021/ic1021164 |*Inorg. Chem.* 2011, 50, 5417–5429

Table 4. Comparison among Shortest Eu−H Distances (nm) in Selected Complexes[a]

complex/type	Phen[b]	CH-β-DK[c]	closest-residue[d]	next closest-residue[d,e]
$Eu(TTA)_3Phen$	0.350(2)/0.552(2)	0.476(3)	0.646(3)	0.662(4)
$Eu(Br\text{-}TTA)_3Phen$	0.344(2)/0.550(2)	0.471(3)	0.621(3)	0.651(4)
$Eu(DTDK)_3Phen$	0.346(2)/0.552(2)	0.470(3)	0.628(6)	0.651(4)
$Eu(MeT\text{-}TTA)_3Phen$	0.333(2)/0.551(2)	0.467(3)	0.609(3)	0.639(4)

[a] H-atoms are conventionally placed at 0.093 nm to the carbon to which they are bonded. Only the average values less than 0.7 nm are considered. The average contact number is indicated in parentheses. For the H-type see Scheme 3. [b] H-atoms belonging to Phen residues (H1, H2). [c] H-atom of three β-DK moieties (H3). [d] H-atoms of thienyl rings (H4). [e] H-atom of Phen residues (H5).

The range of Eu−O distances is comprised within 3σ (line 2 of Table 3), hence fairly significant, while the range of Eu−N distances exceeds 6σ (line 3 of Table 3), clearly meaningful. Specifically the Eu−N distances enlarge in the case of short Eu−Eu contacts, as detected in $Eu(MeT\text{-}TTA)_3Phen$ characterized by very loose crystal-packing.

However, a clear correlation with photophysical behavior of TTA type Eu(III) complexes cannot be evinced; hence, we conceived the angles between mean molecular planes involving EuOO and β-DK residues, which map the juxtaposition of molecular orbitals (MO) raised from ligand field theory of f electrons of the Eu atom with the lone pair n-orbitals of the ligand oxygen atoms.[35] This determines the effectiveness of the ET between metal to ligand or vice versa, even in the case of distorted octahedral coordination. Specifically the a_{2u} MO antibonding of Eu(III) will overlap with the n-orbitals of oxygen of the β-DK groups linked to the metal, and such a superimposition is as efficient as small are the angles between the planes. In lines 5−7 of Table 3 such values are reported for selected complexes.

It is evident that in the case of the $Eu(TTA)_3Phen$ complex the sum of the angles is clearly reduced (<15°) while in all the other compounds, the value exceeds 25°, clearly indicating a different electronic environment to the metal, that is, less efficient overlapping of f (Eu) and n (O) orbitals.

Finally a crucial effect onto emission properties has been checked, namely, the distance of the aromatic H atoms from the metal and the number of such contacts.[31b] In Table 4 such relevant distances, lower than 0.7 nm, are reported for selected crystal structures of Eu(III) complexes. The H atoms were considered conventionally at 0.093 nm from the carbon atom to which they are bonded. Different types are distinguished in Scheme 3, with the label corresponding to the column of Table 4.

The number of aromatic-H contacts, playing a relevant role in quenching the complex emission, is indicated in parentheses for each H-type. In all crystal structures examined the closest Eu−H contacts involve H atoms near to Phen N-atoms (column 2 of Table 4); however other significant contacts should be considered, that is, the H atom of the β-DK residue (column 3 of Table 4) and the H atom of the thienyl ring closer to the β-DK group (column 4 of Table 4). The other closer contacts are indicated in column 5 of Table 4. According to different chemical constitution of the ligands, the number of such contacts changes, namely, it doubles when the CF_3 group is substituted by a thienyl residue.

Indeed only an accurate analysis permits to extract significant differences to evince any trend, that is a reduction of distances of type 3, 4, and 5 is observed comparing the first, second, and fourth complexes, while the type 4 number of contacts is doubled in the third compound with respect to $Eu(TTA)_3Phen$. Hence the effectiveness of aromatic-H quenching should be augmented, consistent with the trend of measured PL-QY (see optical section). However, for the third complex and for $Eu(MeT\text{-}TTA)_3Phen$ the main cause of PL-QY decrease should be attributed to the reduced ET related to the corresponding ligand triplet state energy. In fact, moving from solid state to solution no variation of PL-QY value can be observed. In summary, both the angles between planes (Table 3) and H−Eu distances (Table 4) can tune the observed variation of PL-QY in the selected complexes.

Scheme 3

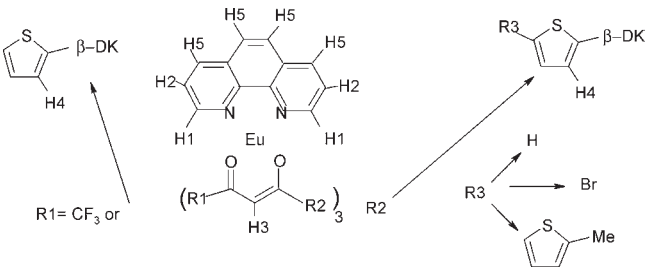

Solution NMR Analysis. The ^1H NMR spectrum of $Eu(TTA)_3Phen$ (see Scheme 4 for the numbering) in $CDCl_3$ solution consists of eight reasonably narrow lines displaying a moderate paramagnetic shift (on the average about 1.5 ppm), allowing for the immediate assignment based on the coupling patterns of thiophene and Phen.

The presence of one set of signals is at odds with the XRD geometry, where the complex displays C_1 symmetry and consequently the three TTA ligands should give rise to different sets of signals. Lowering the temperature to −40 °C did not lead to significant line-broadening, which suggests a static structural rearrangement leading to a real C_3 structure, rather than a dynamic process. To gain insight into the geometry of this system, we decided to switch to lanthanides inducing larger paramagnetic shifts. The rationale for doing so is that a dynamic process which appears fast on the time scale dictated by the small paramagnetic shifts induced by Eu(III) may become slow or at least intermediate for a lanthanide spreading the signals over a much wider range. The first choice in this respect was Tb(III), which is reasonably close to Eu(III), but is associated to a much larger magnetic anisotropy.[36−38] As expected, the ^1H spectrum spans a much wider range, from −30 to +23 ppm with some line broadening, which is anyway not too severe, given the relaxation properties of this ion (the broadest line has a width less than 150 Hz, but there are two lines less than 15 Hz wide), which once more points against the dynamic rearrangement. We may recall that at 14.1 T, the expected line-width of a proton separated by 0.5 nm from Tb(III), in a complex of size comparable to the present ones, is around 210 Hz.[38]

dx.doi.org/10.1021/ic1021164 |Inorg. Chem. 2011, 50, 5417–5429

Scheme 4

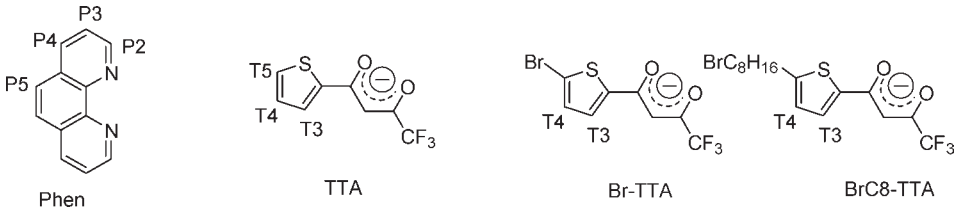

Because this matter appeared of great relevance for understanding the geometry of the red-emitting species in solution, we prepared a series of Ln(TTA)$_3$Phen, with Ln = La, Pr, Eu, Tb, Tm, Yb, and Lu, and measured ^{1}H spectra and longitudinal relaxation times T_1 on all of them (Supporting Information, Table S6). In no case did we observe more than the expected 8 signals, but sometimes we could not identify some. While the assignment of the diamagnetic species together with Eu was straightforward, because of the coupling and chemical shift patterns, for the other paramagnetic systems we took advantage of the longitudinal relaxation rates, as described below, and verified this assignments with two-dimensional (2D) correlation (COSY) for Yb and Pr.

In paramagnetic systems, when one can exclude chemical exchange and contact relaxation, nuclear relaxation is affected and often dominated by two interactions, dipolar and Curie terms.[39] These two mechanisms provide terms to the observed relaxation rate ρ^{obs}, that add up to what can be regarded as an intrinsic diamagnetic term ρ^{dia}, which is what one would have in the absence of paramagnetism and can be very appropriately estimated through the diamagnetic La or Lu analogues. Both dipolar and Curie terms contain an explicit dependence to the nucleus-Ln^{3+} distance, r, and are proportional to $1/r^6$. Thus the observed relaxation rate can be written as

$$\rho^{obs} = \rho^{dia} + \rho^{dipolar} + \rho^{Curie} = \rho^{dia} + \frac{\text{const}}{r^6} \qquad (1)$$

where the constant in the last term depends on the electronic and reorientational correlation times but can ultimately be treated as a heuristic parameter to be fitted. The above equation holds for both longitudinal and transverse rates.

To assign the spectrum of a paramagnetic Ln(TTA)$_3$Phen (Ln = Pr, Tb, Tm, Yb), in a very first approximation, we neglected the diamagnetic term ρ^{dia} and tentatively postulated isostructurality. In this case, the i-th proton in the various complexes with different Ln would have the same distance r from Ln, and the paramagnetic longitudinal relaxation rate for proton i, in the complex with Ln, $\rho_i^{para}(Ln)$, would be proportional to the one of the Eu complex. With all these approximations, we may expect

$$\rho_i^{obs}(\text{Ln}) \propto \rho_i^{obs}(\text{Eu}) \qquad (2)$$

For each complex with a certain Ln, we sorted the observed rates in ascending order, and we could immediately verify the proportionality with the data obtained for Eu. This procedure leads to linear plots of ρ_i^{obs}(Ln) vs ρ_i^{obs}(Eu) (Supporting Information, Figure S5−S8). This simple fact demonstrates two important things: (1) chemical exchange (as well as other mechanisms) can be ruled out as a source of longitudinal relaxation; (2) from the point of view of Ln−H distances, the complexes are isostructural.

Table 5. Observed ^{1}H and ^{13}C Shifts[a] and Longitudinal Relaxation Rates (s^{-1}) for Yb(TTA)$_3$Phen and Lu(TTA)$_3$Phen

	^{1}H				^{13}C	
position	δ^{Yb}	δ^{Lu}	ρ_1^{Yb}	ρ_1^{Lu}	δ^{Yb}	δ^{Lu}
T3	3.53	7.57	21.3	0.57	123.1	129.8
T4	5.89	7.02	2.5	0.44	126.0	127.9
T5	6.93	7.49	2.5	0.31	130.5	132.4
CH	−10.2	6.12	40.0	0.55	56.3	92.3
P2	3.8	9.67	>100	0.61	ND	151.8
P3	12.8	7.81	18.2	0.60	136.0	ND
P4	18.2	8.37	10.6	0.61	155.3	137.6
P5	19.3	7.82	8.4	0.61	144.8	125.8

[a] Parts per million (ppm) referred to the residual solvent signal at 7.26 ppm and 77.0 ppm, respectively.

As a side observation we can mention that indeed ρ^{dia} plays a minor role.

This procedure allowed us to assign the proton resonances. Only proton 2 on Phen here indicated as P2 is elusive, but in fact it appears broadened not only in Eu, but also in La and Lu spectra.

Once this assignment was made, we verified it for Pr and Yb, by homonuclear correlation (COSY) (Table 5 and Supporting Information, Figure S9−S10).

The observed shifts allowed us to extract the paramagnetic term, which could be used for a further check of the isostructurality along the series, by plotting $\delta^{para}(\text{Ln})/\langle S_z(\text{Ln})\rangle$. These plots were linear for Ln = Eu−Yb, but not for Pr, which indicates that Pr(TTA)$_3$Phen may have a different structure. This, put together with the observation made above of proportionality in the relaxation rates, may be interpreted with a different coordination number because of different axial ligation for Pr. Since anyway we were interested in the Eu complex, we did not further investigate the lighter lanthanide.

The separation of contact and pseudocontact terms was attained by means of Reilley's method on the data for Eu−Yb, and the pseudocontact shifts (δ^{PC} or PCS) were used for structural optimization, together with the relaxation rates by means of the program PERSEUS.[38] As the diamagnetic reference, we used the data of Lu(TTA)$_3$Phen.

Since we know that there is a structural rearrangement leading to C_3 symmetry, it is clear that the X-ray crystal structure cannot be used as the input. Therefore, we optimized separately the TTA part and Phen.

For TTA we could find 4 ^{1}H PCS and 4 longitudinal relaxation rates. The latter ones are fully compatible with the X-ray structure, which means that the location of Ln with respect to the individual

dx.doi.org/10.1021/ic1021164 |Inorg. Chem. 2011, 50, 5417–5429

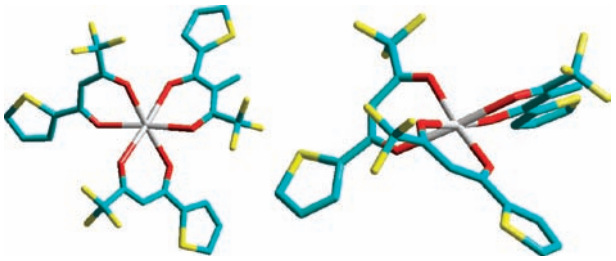

Figure 5. Optimized structure for the $Ln(TTA)_3$ portion in solution based on the analysis of paramagnetic NMR data. Left: view from the top (along the C_3 axis); right: view from the side. Phen moiety is omitted for clarity.

β-DK is correct to the best of our paramagnetic NMR data. Because the complex is axially symmetrical, the magnetic anisotropy is fully described by one parameter D and two Euler angles defining the orientation of this rod-shaped anisotropy with respect to the ligand. These two parameters were optimized through PERSEUS, affording the structure of the $Ln(TTA)_3$ moiety represented in Figure 5.

For the Phen ligand we identified only 3 PCS because protons P2 and P3 were not detected with certainty in the Tb spectrum; on the other hand, because P3 was clearly seen in Eu, Tm, and Yb, we could use its relaxation rate, as well. For symmetry reasons, Phen must lie exactly on the C_3 axis; thus, in principle the parameters D and angle θ determined above should completely fit the experimental data, which appeared unsatisfactory, leading to an agreement factor $R > 9\%$. Accordingly, the geometry was allowed to vary, by changing the distance of the ligand from Ln, while maintaining it along C_3. By so doing a good solution was found, where the ligand is moved 0.04 nm away from Ln.

All of the above findings may suffer of the very limited number of experimental data because of the few protons in the ligands. Observing that the contact shifts for Yb are usually small and that they anyway provide a contribution to the total paramagnetic shift which is scattered in magnitude and sign, we decided to neglect it altogether, but at the same time to take full advantage of the ^{13}C shifts, as well, as determined by heteronuclear correlation. The result is not significantly different from what was found above and is summarized in Tables 6 and 7.

We moved on to study the complex including the brominated ligand Br-TTA shown in Scheme 4. In this case we focused only on the Yb system. By mixing 1 equiv of Br-TTA with 2 equiv of TTA during the synthesis of the complex, we obtained a perfectly statistical distribution of the species incorporating 0,1,2,3 brominated units. These are most easily identified by monitoring the C−H resonances, which are the most spread. No exchange between these forms in the time scale of our EXSY spectra (100 ms) takes place. Although a detailed analysis is rather involved, the observed shifts are compatible with the structure described above for *all* of the complexes of this mixture. The spread in the observed shifts has to be attributed only to a modest difference in the constant D, but we are presently unable to speculate on its origin.

The situation is not much different for the complex incorporating three alkylated TTA units in Ln (BrC8-TTA)$_3$Phen.

As a conclusion, $Ln(TTA)_3$Phen in $CHCl_3$ solution, as well as the derivatives containing brominated or alkylated TTA, must be depicted as undergoing a major structural rearrangement with respect to the crystal state, leading to a real C_3 symmetry of the TTA portion and with the ligand Phen capping the distorted trigonal antiprism of the 6 oxygen atoms of TTA ligands. The Ln−Phen distance is somewhat elongated (e.g., Yb−N attains a value of 0.286 nm). It is interesting to observe that by means of EXSY experiments we observed that there is exchange between free and bound Phen. This process is slow on the time scale of the paramagnetic spectrum provided by Yb, that is, neither shift nor relaxation rates of the bound form are affected by this exchange. On the contrary, TTA is firmly bound to the lanthanide.

Table 6. Experimental Total Paramagnetic Shifts and Calculated PCS for $Yb(TTA)_3$Phen, Relative to the $Yb(TTA)_3$ Moiety Only[a]

	position	δ^{para}(exp)	δ^{pc}(calc)
^1H	T3	−4.04	−4.18
	T4	−1.13	−1.51
	T5	−0.56	−1.95
	CH	−16.32	−11.8
^{13}C	T3	−6.7	−5.18
	T4	−1.9	−2.63
	T5	−1.9	−2.86
	CH	−36	−37.75

[a] The agreement factor $R = 1.8\%$; the magnetic anisotropy constant D = 2200 (200) ppm Å^3.

Table 7. Experimental Total Paramagnetic Shifts and Calculated PCS for $Yb(TTA)_3$Phen, Relative to the $Yb(Phen)_3$ Moiety Only[a]

	position	δ^{para}(exp)	δ^{pc}(calc)
1H	P3	4.99	1.23
	P4	9.83	8.41
	P5	11.48	10.80
13C	P4	17.70	14.30
	P5	19.00	17.29

[a] The Yb-Phen distance was allowed to change and increased by 0.4 Å, with respect to the x-ray structure, while the magnetic anisotropy constant D was kept fixed at the value found above (D = 2200 ppm Å^3). Agreement Factor $R = 3.4\%$.

PL-QY Correlation. Optical and structural characterizations strongly address the ranking of PL-QY in the series of complexes both in solid state and in solution. XRD solid state structural determination and solution paramagnetic NMR experiments contribute to deepen the knowledge of TTA Eu complexes, particularly they evidence along the series a change of symmetry and a variation of the Eu-ligand distances below 0.05 nm moving from solution to solid state. Moreover, fine structure details in crystal structures reveals that the number of H-atom near to Eu(III) ion together with the angle between EuOO and diketonate planes strongly affect the Eu emission, namely, the increase of both factors largely contributes to luminescence quenching.

In solution, paramagnetic NMR shows that the symmetry level increases, producing a decrease of $Eu(TTA)_3$Phen PL-QY although the accuracy of their determination prevents an appreciation of how the Eu−ligand distances vary along with the TTA series; hence, we cannot fully correlate these with the different nonradiative (A_{NR}) decay rates calculated for TTA complexes.

dx.doi.org/10.1021/ic1021164 |*Inorg. Chem.* 2011, 50, 5417–5429

CONCLUSIONS

A series of Eu(III) complexes based on the β-diketonate moiety was prepared, studied in detail, and compared with analogous compounds already known. Steady-state and time-resolved emission spectroscopy, overall PL-QY measurements, intimate fine structural features determined by XRD crystal structure, molecular modeling, and solution paramagnetic NMR analysis allowed us to justify the PL-QY ranking in the series both in solid state and in solution. While for β-diketonate complexes containing more thiophene rings the energy of the ligand triplet state explains the measured values of PL-QY, for the TTA type complexes finer consideration must be considered on the quenching due to the coupling of the Eu(III) excited state with the second overtone of proximate aromatic C−H oscillators (ν_{CH} ~3050 cm^{-1}).

ASSOCIATED CONTENT

Supporting Information. Synthesis of the ligands, cyclovoltammetric data, phosphorescence spectra of frozen solution of Gd(III) complexes, photoluminescence spectra of complexes in solid state, analysis of crystals of Eu (III)-Complexes based on β-DK/Phenanthroline type ligands, solution NMR analysis, and CIF files of crystal structures. This material is available free of charge via the Internet at http://pubs.acs.org.

AUTHOR INFORMATION

Corresponding Author
*E-mail: s.destri@ismac.cnr.it.

ACKNOWLEDGMENT

The work has been partially supported by PRIN 2007 project 2007PBWN44 of Italian MIUR

REFERENCES

(1) Bünzli, J-C. G.; Piguet, C. *Chem. Soc. Rev.* **2005**, *34*, 1048.
(2) Kido, J.; Okamoto, Y. *Chem. Rev.* **2002**, *102*, 2357.
(3) Hasegawa, Y.; Wada, Y.; Yanagida, S. *J. Photochem. Photobiol., C* **2004**, *5*, 183.
(4) (a) Montalti, M.; Prodi, L.; Zaccheroni, N.; Charbonniere, L.; Douce, L.; Ziessel, R. *J. Am. Chem. Soc.* **2001**, *123*, 12694. (b) Tsukube, H.; Shinoda, S. *Chem. Rev.* **2002**, *102*, 2389.
(5) (a) Eliseevaa, S. V.; Bünzli, J-C. G. *Chem. Soc. Rev.* **2010**, *39*, 189. (b) Escribano, P.; Lopez, B. J.; Planelles-Arago, J.; Cordoncillo, E.; Viana, B.; Sanchez, C. *J. Mater. Chem.* **2008**, *18*, 23, and references therein.
(6) Klink, S. I.; Grave, L.; Reinhoudt, D. N.; van Veggel, F. C. J. M.; Werts, M. H. V.; Geurts, F. A. J.; Hofstraat, J. W. *J. Phys. Chem. A* **2000**, *104*, 5457.
(7) (a) de Bettencourt-Dias, A. *Dalton Trans.* **2007**, *22*, 2229. (b) Giovanella, U.; Pasini, M.; Freund, C.; Botta, C.; Porzio, W.; Destri, S. *J. Phys. Chem. C* **2009**, *113*, 2290. (c) Law, G. L.; Wong, K. L.; Tam, H. L.; Cheah, K. W.; Wong., W. T. *Inorg. Chem.* **2009**, *48*, 10492. (d) Katkova, M. A.; Balashova, T. V.; Ilichev, V. A.; Konev, A. N.; Isachenkov, N. A.; Fukin, G. K.; Ketkov, S. Y.; Bochkarev, M. N. *Inorg. Chem.* **2010**, *49*, 5094.
(8) (a) Moudam, O.; Rowan, B. C.; Alamiry, M.; Richardson, P.; Richards, B. S.; Jones, A. C.; Robertson, N. *Chem. Commun.* **2009**, 6649. (b) Raj, D. B. A; Francis, B.; Reddy, M. L. P.; Butorac, R. R.; Lynch, V. M.; Cowley, A. H. *Inorg. Chem.* **2010**, *4*, 9055. (c) Hasegawa, Y.; Kawai, H.; Nakamura, K.; Yasuda, N.; Wada, Y.; Yanagida, S. *J. Alloys Compd.* **2006**, *408*, 669. (d) Hasegawa, Y.; Yamamuro, M.; Wada, Y.; Kanehisa, N.; Kai, Y.; Yanagida, S. *J. Phys. Chem. A* **2003**, *107*, 1697. (e) Kuriki, K.; Koike, Y.; Okamoto, Y. *Chem. Rev.* **2002**, *102*, 2347.
(9) (a) Piguet, C.; Bünzli, J.-C. G. *Chem. Soc. Rev.* **1999**, *28*, 347. (b) Binnemans, K. *Chem. Rev.* **2009**, *109*, 4283.
(10) (a) Robinson, M. R.; Osrtowsky, J. C.; Bazan, G. C.; McGehee, M. D. *Adv. Mater.* **2003**, *15*, 1547. (b) Liang, F. S.; Zhou, Q. G.; Cheng, Y. X.; Wang, L. X.; Ma, D. G.; Jing, X. B.; Wang, F. S. *Chem. Mater.* **2003**, *15*, 1935.
(11) (a) Chauvin, A.; Gumy, F.; Matsubayashi, I.; Hasegawa, Y.; Bünzli, J-C. G. *Eur. J. Inorg. Chem.* **2006**, 473. (b) Yu, J.; Zhou, L.; Zhang, H.; Zheng, Y.; Li, H.; Deng, R.; Peng, Z.; Li, Z. *Inorg. Chem.* **2005**, *44*, 1611.
(12) Malta, O. L.; Brito, H. F.; Menezes, J. F. S.; Goncalves e Silva, F. R.; Donega, C. D.; Alves, S. *Chem. Phys. Lett.* **1998**, *282*, 233.
(13) de Sá, G. F.; Malta, O. L.; de Mello Donegá, C.; Simas, A. M.; Longo, R. L.; Santa-Cruz, P. A.; da Silva, E. F., Jr. *Coord. Chem. Rev.* **2000**, *196*, 165.
(14) Glover, P. B.; Bassett, A. P.; Nockemann, P.; Kariuki, B. M.; Van Deun, R.; Pikramenou, Z. *Eur. J.* **2007**, *13*, 6308.
(15) Farrugia, L. J. *J. Appl. Crystallogr.* **1999**, *32*, 837.
(16) Moreau, J.; Giovanella, U.; Bombenger, J.-P.; Porzio, W.; Vohra, V.; Spadacini, L.; Di Silvestro, G.; Barba, L.; Arrighetti, G.; Destri, S.; Pasini, M.; Saba, M.; Quochi, F.; Mura, A.; Bongiovanni, G.; Fiorini, M.; Uslenghi, M.; Botta, C. *Chem. Phys. Chem.* **2009**, *10*, 647, and references therein.
(17) Southard, G. E.; Murray, G. M. *J. Org. Chem.* **2005**, *70*, 9036.
(18) Okada, K.; Wang, Y.-F.; Chen, T.-M.; Kitamura, M.; Nakaya, T.; Inoue, H. *J. Mater. Chem.* **1999**, 3023.
(19) Sambasivarao, K.; Dhurke, K.; Kakali, L.; Raghavan, B. S. *Eur. J. Org. Chem.* **2004**, *19*, 4003.
(20) Michalitsch, R.; Lang, P.; Yassar, A.; Nauer, G.; Garnier, F. *Adv. Mater.* **1997**, *9*, 321.
(21) Back, N. S.; Kim, Y. H.; Eom, Y. K.; Oh, J. H.; Kim, H. K.; Aebischer, F. G.; Chauvin, A. S.; Bünzli, J-C. G. *Dalton Trans.* **2010**, *39*, 1532.
(22) Melby, L. R.; Rose, N. J.; Abramson, E.; Caris, J. C. *J. Am. Chem. Soc.* **1964**, *86*, 5117.
(23) Goncalves e Silva, F. R.; Longo, R.; Malta, O. L.; Piguet, C.; Bunzli, J-C. G. *Phys. Chem. Chem. Phys.* **2000**, *2*, 5400.
(24) Chen, Z.; Ding, F.; Hao, F.; Guan, M.; Bian, Z.; Ding, B.; Huang, C. *New J. Chem.* **2010**, *34*, 487.
(25) Sato, S.; Wada, M. *Bull. Chem. Soc. Jpn.* **1970**, *43*, 1955.
(26) Venchikov, V. Ya.; Tsvirko, M. P. *J. Appl. Spectrosc.* **2001**, *68*, 6.
(27) Binnemans, K. In *Handbook on thePhysics and Chemistry of Rare Earths*; Gschneidner, K. A. Jr., Bünzli, J.-C. G., Pecharsky, V. K., Eds.; Elsevier: Amsterdam, The Netherlands, 2005; Vol. 35, Chapter 225, p 107.
(28) Shavaleev, N. M.; Eliseeva, S. V.; Scopelliti, R.; Bünzli, J-C. G. *Inorg. Chem.* **2010**, *49*, 3927.
(29) Bunzli, J-C. G. In *Lanthanide Probes in Life,Chemical and Earth Sciences, Theory and Practice*; Bunzli, J-C. G., Choppin, G. R., Eds.; Elsevier: New York, 1989; p 219.
(30) Kirby, A. F.; Foster, D.; Richardson, F. S. *Chem. Phys. Lett.* **1983**, *95*, 507.
(31) (a) Kropp, J. L.; Windsor, M. W. *J. Chem. Phys.* **1965**, *42*, 1599. (b) Beeby, A.; Clarkson, I. M.; Dickins, R. S.; Faulkner, S.; Parker, D.; Royle, L.; de Sousa, A. S.; Williams, J. A. G.; Woods, M. *J. Chem. Soc., Perkin Trans. 2* **1999**, 493.
(32) Hu, M.; Huang, Z. H.; Cheng, Y. Q.; Wang, S.; Lin, J. J.; Hu, L.; Xu, D. J.; Xu, Y. Z. *Chin. J. Chem.* **1999**, *17*, 637.
(33) Hui-Biao, L.; Bao-Long, L.; Hua-Qin, W.; Zheng, X. *Chin. J. Chem.* **2001**, *19*, 766.
(34) *MATSTUDIO*, modeling release 4.0; Accelrys Inc:. San Diego, CA, 2003 (www.accelrys.com).
(35) See, for example, Atanasov, M.; Daul, C.; Guldel, H. U.; Wesolowski, T. A.; Zbiri, M. *Inorg. Chem.* **2005**, *44*, 2954.
(36) Bleaney, B. *J. Magn. Reson.* **1972**, *8*, 91.
(37) Mironov, V. S.; Galyametdinov, Y. G.; Ceulemans, A.; Gorller-Walrand, C.; Binnemans, K. *J. Chem. Phys.* **2002**, *116*, 4673.
(38) Di Bari, L.; Salvadori, P. *Coord. Chem. Rev.* **2005**, *249*, 2854.
(39) Bertini, I.; Luchinat, C. *Coord. Chem. Rev.* **1996**, 150.